Thin Solid Films 722 (2021) 138573

Contents lists available at ScienceDirect

Thin Solid Films

journal homepage: www.elsevier.com/locate/tsf

Deposition and characterization of lithium doped direct current magnetron sputtered Cu_2O films

M. Nyborg *, A. Azarov, K. Bergum, E. Monakhov

Department of physics, center of Materials Science and Nanotechnology, University of Oslo, PO Box 1048, Blindern, N-0316 Oslo, Norway

ARTICLE INFO

Keywords:
Cuprous oxide
Lithium doping
Reactive sputtering
Optical properties
Electrical properties

ABSTRACT

Lithium doped cuprous oxide ($Cu_2O:Li$) films were deposited on quartz substrates by direct current magnetron reactive co-sputtering of copper and $Cu:Li$ targets. X-ray diffraction (XRD), secondary ion mass spectrometry (SIMS), Rutherford backscattering spectrometry, UV-VIS transmittance, and room temperature Hall measurements have been conducted to characterize the deposited films. SIMS revealed Li concentrations in the range $2\times10^{18}-5\times10^{20}\,cm^{-3}$ in the doped films. XRD confirms phase pure Cu_2O for all doping concentrations. The doping concentration correlates with an increased free carrier density found from Hall effect measurements. The highest Li doping concentration results in low resistivity (4 Ωcm) p-type Cu_2O with acceptor concentrations up to $2\times10^{17}\,cm^{-3}$.

1. Introduction

Cu_2O is a p-type semiconductor with a direct bandgap of 2.1 eV and a high absorption coefficient. It is stable, abundant, non-toxic and has the potential for low cost production schemes [1]. Cu_2O single junction solar cells have a theoretical efficiency of 19% [2]. Minami et al. has shown steep progress with a record efficiency of 8.1% in a bulk Cu_2O absorber based device [3]. Further, the band gap makes Cu_2O a candidate material for tandem solar cells, with an intriguing possibility as the top cell paired with a silicon bottom cell [4].

Cu_2O can be deposited by most thin-film methods, e.g., electrodeposition [5], molecular beam epitaxy [6], atomic layer deposition [7], radio frequency (RF) [8] and direct current (DC) reactive magnetron sputtering [9]. Magnetron sputtering and electrodeposition are most common in solar cell applications and is scalable for large scale production. Many known metal oxide semiconductors' are prone to low-charge carrier lifetimes and carrier mobilities. This is especially valid in sputtered Cu_2O based devices, which have yet to surpass efficiencies of 2-3% [10]. In Cu_2O, this is likely due to poor defect control and low mobility, which results in the inability to control the p-type nature of Cu_2O. The p-type conductivity is generally accepted to be due to persistent intrinsic acceptor states of copper vacancies (V_{Cu}), and so-called split-vacancies (V_{Cu}^{Split}) [11–18].

Doping of Cu_2O is widely explored, with transition metals, hydrogen, silicon, nitrogen, and more [19]. Most notably are the properties of nitrogen-doped p-type Cu_2O, with low resistivity and the possibility of tuning the electrical properties of Cu_2O [9,20]. There are no reports of viable routes to n-type conductivity in sputtered Cu_2O films, and most dopants lead to an increase in acceptor concentration. Isseroff and Carter [18] presented Lithium (Li) as an isovalent substitutionary cation with similar ionic size of Li^+ as that of Cu^+. Density functional theory calculations suggest that Li doping can form $V_{Cu}-Li$ complex in Cu_2O. The optimal defect complex structure was identified as Li tetrahedrally coordinated to four oxygen atoms, similar to V_{Cu}^{split}, resulting in a large driving force to cluster [18]. Besides, Li at the interstitial site (Li_i) can be expected to act as a donor. Thus, Li could be a route to passivate the high acceptor density in Cu_2O.

There is little literature on the effect of Li doping of Cu_2O, with only a few studies reporting increased carrier concentrations and increased conductivity in doped films [5,21,22]. In this work we investigate the effect of Li doping with varied concentrations in Cu_2O. Cu_2O films were deposited on quartz substrates by reactive co-sputtering of pure copper, 1% and 0.01% Li doped copper targets. Characterization of the films was carried out by X-ray diffraction (XRD), secondary ion mass spectrometry (SIMS), Rutherford backscattering spectrometry (RBS), UV-VIS transmittance, and room temperature Hall measurements (RTH).

2. Experimental details

Cu_2O films were deposited on 1×1 cm^2 fused silica substrates (t =

* Corresponding author.

https://doi.org/10.1016/j.tsf.2021.138573
Received 7 May 2020; Received in revised form 11 January 2021; Accepted 4 February 2021
Available online 9 February 2021

500 μm) by reactive DC and RF magnetron co-sputtering in a Semicore Triaxis system. The fused silica substrates were cleaned for 1 min in Pirhana solution, rinsed in DI water, and subsequently ultrasonically washed in isopropanol for 5 min. The base pressure in the deposition chamber was below 2.7×10^{-4} Pa (2×10^{-6} Torr). Before deposition, the targets were pre-sputtered for 20 min, and then films were deposited for $\simeq$ 15 min at 400 °C. The samples were made with Cu (4N, AEM inc), CuLi (99:1 wt% AEM inc), and Cu:Li (99.99:0.01 wt% AEM inc) targets with varying powers on DC and RF to achieve different lithium content. A series of samples were deposited with varying oxygen flow for each batch to achieve optimal growth conditions and phase pure Cu_2O. The sum of oxygen and argon mass flow rate was fixed at 50 sccm. Table 1 contains detailed deposition parameters of the five phase-pure Cu_2O samples with varying Li content selected for further characterization.

Structural and compositional analysis was performed by a combination of XRD, SIMS, and RBS. XRD was performed on a Bruker AXS D8 Discover system, Cu Kα_1 radiation ($\lambda = 1.54$ Å) scanned over the angles 20° to 80° 2θ. SIMS measurements were done in a Cameca IMS7f microanalyzer with O_2^+ primary ions at 10 keV. RBS analysis was performed with 1.62 MeV $4He^+$ ions backscattered into a detector placed at 165° relative to the incident beam direction. Analysis of the RBS spectra was performed using simulation with the SIMNRA code [23]. Optical data were obtained from transmission measurements employed in the spectral range of 290-2500 nm with an integrating sphere on a Shimadzu SolidSpe-3700 DUV spectrophotometer. RTH was performed in a Lake-Shore 7604 setup in the Van-der Pauw configuration. Contacts were prepared by soldering Ag wires onto the samples' corners with indium (contact size, $d \simeq 1\,mm$).

3. Results and discussion

XRD patterns in Fig. 1 indicate that all films are crystalline and single-phase Cu_2O with no detectable peaks from CuO or Cu. All samples except #4 are dominated by the Cu_2O 111 reflection at 36.5°. In sample #4, both the 111 reflection and 200 reflection at 42.3° are similarly visible, indicating a less directional growth along the [111] direction. Cu_2O preferred growth orientation is sensitive to O_2 partial pressure and total pressure during deposition [24,25]. O_2 flow was adjusted for each sample to suit the target configuration and power applied for the different Li concentrations. The difference in the preferred orientation of sample #4 is likely due to the lower oxygen partial pressure during deposition. Measurement of clean fused silica substrate was performed to rule out background peaks, and these are marked by asterisk in Fig. 1. The crystallite size is estimated by the Scherrer's formula given by Dastan et al. [26], Dastan [27], Dastan et al. [28], Jafari et al. [29], Zhou et al. [30]:

Table 1
Deposition parameters during the growth of the Cu_2O films.

Sample	#1	#2	#3	#4	#5
Cu target	DC 100 W	-	DC 100W	DC 100W	-
Cu : *Li* target [99.99/ 0.01 wt%]	-	DC 100 W	-	-	-
Cu : *Li* target [99/1 wt %]	-	-	RF 10W	RF 50W	DC 100W
Argon flow [sccm]	40.5	41	44.7	45.5	44.5
Oxygen flow [sccm]	9.5	9.0	5.3	4.5	5.5
Temperature [°C]	400	400	400	400	400
Rotation [RPM]	12	12	12	12	12
Base pressure [1 × 10^{-4}Pa]	2.7	2.7	2.7	2.7	2.7
Deposition time [min]	15	15	15	15	15
Thickness [nm]	290	380	390	470	430

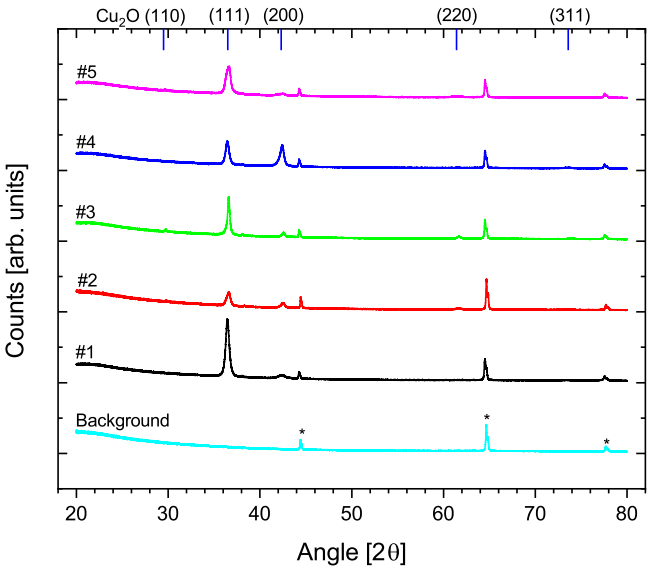

Fig. 1. $\theta - 2\theta$ XRD pattern of Cu_2O (#1) and $Cu_2O : Li$ films with increasing Li content (#2-5). Asterisk mark peaks stemming from the background scan.

$$D = \frac{K\lambda}{\beta Cos\theta} \tag{1}$$

where D is the crystallite size, K the Scherrer constant (0.94), $\lambda = 0.1543\,nm$ the X-ray wavelength, and θ the FWHM from a gaussian fit on the 111 peak in radians. D_p deduced from the 111 peak gives crystallite sizes of 30-50 nanometer for the different films without any apparent doping concentration trend. Slightly larger than the report of 14–20 nm crystallites in RF sputtered Cu_2O films by Gan et al. [8]. The crystallite size deduced from the Scherrer equation should be used cautiously with sputtered films. The equation is designed for spherical powder samples. Non-spherical shape of the crystallites, stress/strain, non-uniform crystallite sizes, and other peak broadening effects will impact the analysis.

Fig. 2 shows the measured optical transmission spectra for wavelengths from 290 to 2500 nm for the Cu_2O and $Cu_2O : Li$ films. The spectra show no apparent features emerging from Li doping, and high optical transmittance of 85-90 % is observed in all samples. High absorption is indicated by the clear decline towards zero transmittance for energies above the lowest allowed optical transitions at $\simeq$ 470 nm ($\Gamma_7^+ \rightarrow \Gamma_8^-$) [1,31]. The interference fringes indicate that sample #1 has a lower thickness than samples #2-5. SIMS measurements (Cu65 signal) confirms this, where sample #1 has a thickness of 290 nm compared to about 400-500 nm for sample #2-5. The study of Malerba et al. found that the absorption coefficient in Cu_2O includes various contributions from direct, forbidden, and indirect transitions, and therefore Tauc analysis is not a reliable way to determine the gap of Cu_2O samples [32]. However, Tauc analysis has been employed to investigate the effects of Li doping in Cu_2O (Fig. 3).The optical band gap was deduced through the relation [33–35]:

$$(h\nu\alpha)^{1/n} = A(h\nu - E_g) \tag{2}$$

where h is Planck's constant, f is the photon frequency, α the absorption coefficient, T the transmittance in %, and A a proportionality constant. In this work, we have used the exponent n equals 1/2 for direct allowed transitions. The deduced optical gaps are listed in Fig. 3, giving a mean optical gap of 2.55 ± 0.1 eV, and there is no significant change in the optical gap with Li doping.

Lithium concentration vs. depth profiles as measured by SIMS are shown in Fig. 4. Significant Li concentrations are detected in all the doped films (#2-5), while the undoped sample, #1, has Li concentration

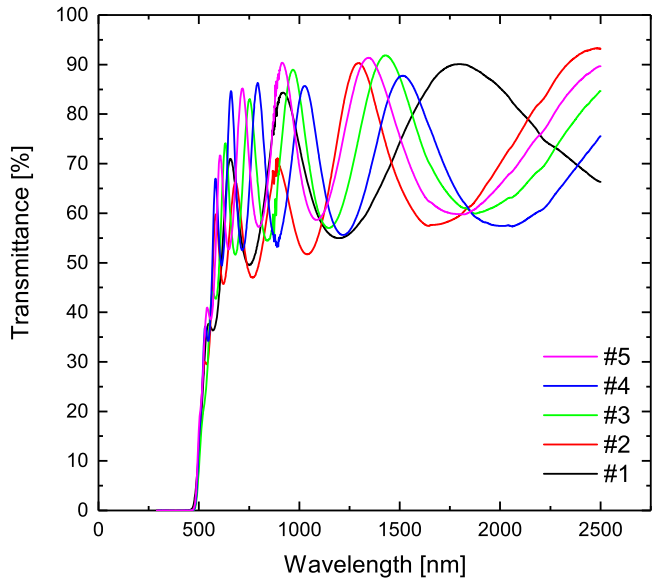

Fig. 2. Transmittance of Cu_2O (#1) and $Cu_2O:Li$ films with increasing Li content (#2-5).

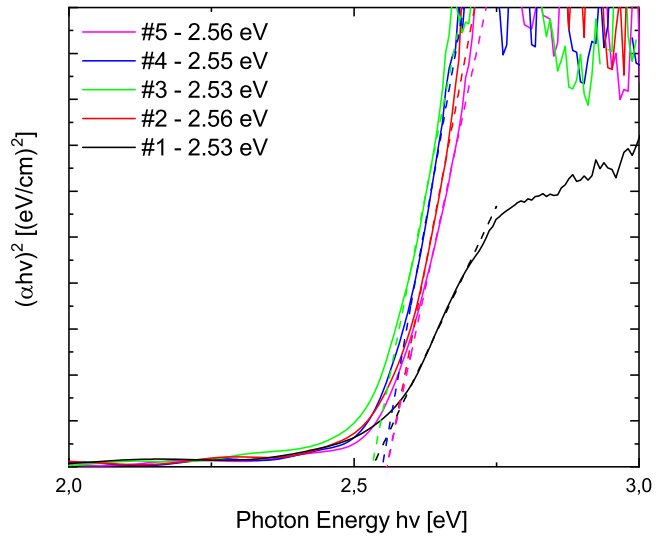

Fig. 3. Tauc plot of the Cu_2O (#1) and $Cu_2O:Li$ films (#2-5) deduced from the transmittance spectra in Fig. 2. The optical bandgap is extracted by extrapolation to the abscissa (dashed lines).

below the detection limit ($< 1 \times 10^{15}\, cm^{-3}$). Samples #2, 3 and 4 have uniform Li distribution throughout the film depth, with average concentrations of $1.9 \times 10^{18}\, cm^{-3}$, $7.0 \times 10^{18} cm^{-3}$, and $2.0 \times 10^{20}\, cm^{-3}$, respectively. It is important to note that in sample #5, there is a Li gradient towards the surface before averaging out at a mean concentration of $5 \times 10^{20}\, cm^{-3}$ after about 80 nm. Also, there is a drop in the copper signal (not shown) towards the surface, corresponding well to the Li-enriched region's depth.

It is believed that Li concentration in the near-surface region may be so high that stoichiometry of this layer is altered, and determination of the exact Li content in this layer may be challenging due to matrix effects. Supporting the SIMS results, the thin O-rich and Cu deficient surface layer formation is also confirmed by RBS results as illustrated by Fig. 5 showing RBS spectra of the undoped (#1) and Li-doped (#5) samples. It might be seen that for sample #5, the Cu edge is shifted towards the lower channels compared to the Cu surface position indicated by the arrow, and there is a small bump in O content (the channels

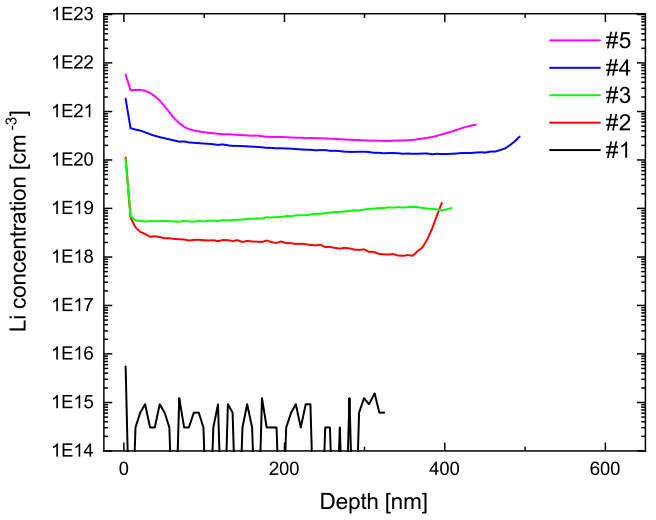

Fig. 4. SIMS depth profiles of the Cu_2O (#1) and $Cu_2O:Li$ films with increasing Li content (#2-5)., with Lithium concentration vs. depth.

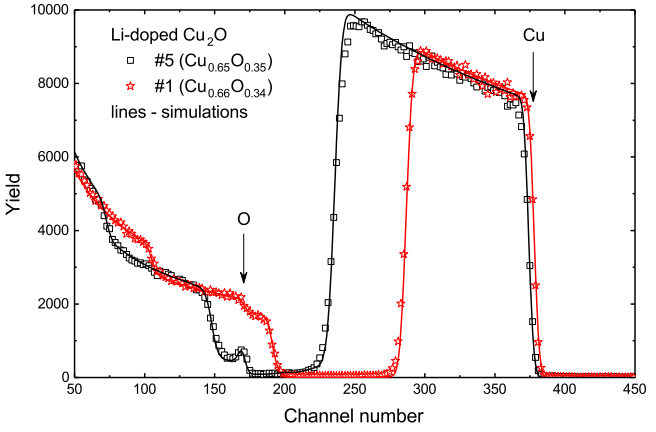

Fig. 5. RBS spectra of the undoped (#1) and Li-doped (#5) Cu_2O films. The surface positions of Cu and O atoms are shown by the arrows. The results of the simulations performed with the SIMNRA code are shown by the solid lines, while the films' obtained composition is plotted in the legend.

165-175). These observations may indicate a formation of a thin oxide layer at the film surface. According to simulations (see the solid line in the figure), the thickness of this layer is estimated to be $\simeq 25\, nm$. It should be noted that although the Li signal is not seen on the RBS spectra due to its low atomic mass, the involvement of Li atoms in this surface layer can not be excluded. According to simulations, the films have a near stoichiometric composition of $Cu_{0.66}O_{0.34}$ and $Cu_{0.65}O_{0.35}$ for samples #1 and #5, respectively. An electrical characterization by RTH measurements was conducted to determine carrier type, density, mobility, and sample resistivity (Fig. 6). The resistivity decreases by 3 orders of magnitude for the samples with high Li content. The decrease in resistivity can be attributed to an increase in acceptor concentration in the highly doped samples. A drop in carrier mobility accompanies this, however mobility above $10\, cm^2/Vs$ is retained in all samples.

The increase in carrier concentration correlates with a high Li concentration in the samples. The origin of the acceptor increase is not clear. Li is an isovalent dopant and not expected to increase the acceptor concentration directly but to passivate acceptor states originating from copper vacancies, i.e. $Li_i^+ + V_{cu}^- \rightarrow Li_{Cu}$, which would lead to a decrease in p-type doping. The high acceptor concentration and previous studies contradict the model where V_{Cu} is the primary defect responsible for the persistent p-type of Cu_2O [5,21,21,22]. One can speculate that

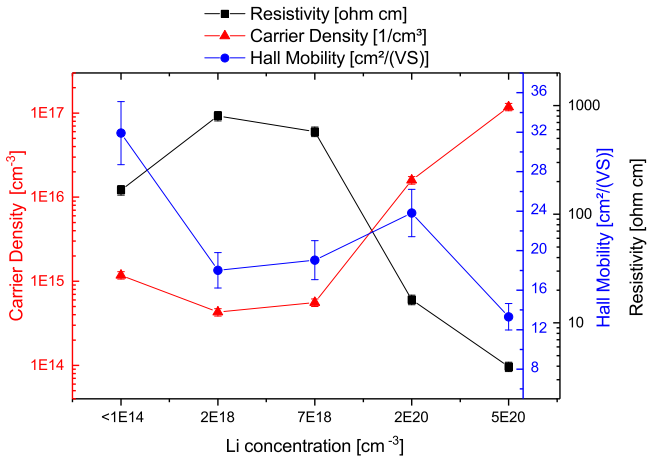

Fig. 6. Resistivity, majority carrier mobility, and carrier concentration as a function of measured lithium concentrations in the films.

hydrogen's role should be considered, similar to the explanations of persistent n-type in ZnO [36,37]. A possible explanation for the increase could be that Li passivates a compensating donor in Cu_2O. This would explain the increase in apparent carrier concentration at room temperature. Finally, one cannot rule out the formation of other unknown defects due to Li doping in Cu_2O.

4. Conclusion

Phase pure Li doped Cu_2O films have been deposited by reactive magnetron co-sputtering of Cu and Cu:Li doped targets. $Cu_2O : Li$ films with Li concentrations of $10^{18} - 10^{21}\ cm^{-3}$ retain their phase, relatively high mobility, and transparency in all investigated samples. However, a thin Cu lean and Li-rich surface layer is observed in the highest doped sample ($\simeq 1wt\%$ Li). The isovalent Li dopant was proposed to reduce acceptor concentration by passivating V_{Cu}. However, increased carrier density with increased Li doping concentrations is observed. The highest doped sample exhibits a high carrier concentration ($1.2 \times 10^{17}\ cm^{-3}$), low resistivity ($4\,\Omega cm$), and mobility of $13\ cm^2/Vs$.

Declaration of Competing Interest

The authors declare that they have no known competing financial interests or personal relationships that could have appeared to influence the work reported in this paper.

Acknowledgments

This work was performed within The Norwegian Research Center for Sustainable Solar Cell Technology (FME SUSOLTECH, project number 257639/E20). The center is co-sponsored by the Research Council of Norway and its research and industry partners. The Research Council of Norway is acknowledged for the support to the Norwegian Micro- and Nano-Fabrication Facility, NorFab, project number 295864.

References

[1] B.K. Meyer, A. Polity, D. Reppin, M. Becker, P. Hering, B. Kramm, P.J. Klar, T. Sander, C. Reindl, C. Heiliger, M. Heinemann, C. Müller, C. Ronning, The physics of copper oxide Cu_2O, in: B.G. Svensson, S.J. Pearton, C. Jagadish (Eds.), Semiconductors and Semimetals vol. 88, Academic Press, 2013, pp. 201–226, https://doi.org/10.1016/B978-0-12-396489-2.00006-0.

[2] W. Shockley, H.J. Queisser, Detailed Balance Limit of Efficiency of p-n Junction Solar Cells, J. Appl. Phys. 32 (3) (1961) 510–519, https://doi.org/10.1063/1.1736034.

[3] T. Minami, Y. Nishi, T. Miyata, Efficiency enhancement using a Zn_{1-x} Ge_x-O thin film as an n-type window layer in Cu_2O-based heterojunction solar cells, Appl. Phys. Express 9 (5) (2016) 052301, https://doi.org/10.7567/APEX.9.052301.

[4] A.D. Vos, Detailed balance limit of the efficiency of tandem solar cells, J. Phys. D. 13 (5) (1980) 839–846, https://doi.org/10.1088/0022-3727/13/5/018.

[5] T.G. Kim, H. Ryu, W.-J. Lee, Effects of lithium (Li) on lithium-cuprous-oxide (Li-Cu_2O) composite films grown by using electrochemical deposition for a PEC photoelectrode, J. Korean Phys. Soc. 68 (2) (2016) 268–273, https://doi.org/10.3938/jkps.68.268.

[6] D.S. Darvish, H.A. Atwater, Epitaxial growth of Cu_2O and ZnO/Cu_2O thin films on MgO by plasma-assisted molecular beam epitaxy, J. Cryst. Growth 319 (1) (2011) 39–43, https://doi.org/10.1016/j.jcrysgro.2011.01.071.

[7] J.R. Avila, A.W. Peters, Z. Li, M.A. Ortuño, A.B.F. Martinson, C.J. Cramer, J. T. Hupp, O.K. Farha, Atomic layer deposition of Cu(i) oxide films using Cu(ii) bis (dimethylamino-2-propoxide) and water, Dalton Trans. 46 (2017) 5790–5795, https://doi.org/10.1039/C6DT02572B.

[8] J. Gan, V. Venkatachalapathy, B. Svensson, E. Monakhov, Influence of target power on properties of Cu_xO thin films prepared by reactive radio frequency magnetron sputtering, Thin Solid Films 594 (2015) 250–255, https://doi.org/10.1016/j.tsf.2015.05.029.

[9] A. Jafari, K. Tahani, S. Asgary, Z. Shi, X.-T. Yin, W.-D. Zhou, H. Garmestani, Ş Ţălu, Ion implantation of copper oxide thin films; statistical and experimental results, Surf. Interfaces 18 (2020) 100463, https://doi.org/10.1016/j.surfin.2020.100463.

[10] T.K.S. Wong, S. Zhuk, S. Masudy-Panah, G.K. Dalapati, Current status and future prospects of copper oxide heterojunction solar cells, Materials 9 (4) (2016) 271, https://doi.org/10.3390/ma9040271.

[11] W.H. Brattain, The copper oxide rectifier, Rev. Mod. Phys. 23 (3) (1951) 203–212, https://doi.org/10.1103/RevModPhys.23.203.

[12] J. Xue, R. Dieckmann, The non-stoichiometry and the point defect structure of cuprous oxide ($Cu_{2-\delta}O$), J. Phys. Chem. Solids 51 (11) (1990) 1263–1275, https://doi.org/10.1016/0022-3697(90)90003-X.

[13] O. Porat, I. Riess, Defect chemistry of $Cu_{2-y}O$ at elevated temperatures. Part II: electrical conductivity, thermoelectric power and charged point defects, Solid State Ionics 81 (1) (1995) 29–41, https://doi.org/10.1016/0167-2738(95)00169-7.

[14] A.F. Wright, J.S. Nelson, Theory of the copper vacancy in cuprous oxide, J. Appl. Phys. 92 (10) (2002) 5849–5851, https://doi.org/10.1063/1.1516620.

[15] G.K. Paul, Y. Nawa, H. Sato, T. Sakurai, K. Akimoto, Defects in Cu_2O studied by deep level transient spectroscopy, Appl. Phys. Lett. 88 (14) (2006) 141901, https://doi.org/10.1063/1.2175492.

[16] M. Nolan, S.D. Elliott, The p-type conduction mechanism in Cu_2O: a first principles study, Phys. Chem. Chem. Phys. 8 (45) (2006) 5350–5358, https://doi.org/10.1039/B611969G.

[17] D.O. Scanlon, B.J. Morgan, G.W. Watson, A. Walsh, Acceptor levels in p-type Cu_2O: rationalizing theory and experiment, Phys. Rev. Lett. 103 (9) (2009) 1–4, https://doi.org/10.1103/PhysRevLett.103.096405.

[18] L.Y. Isseroff, E.A. Carter, Electronic structure of pure and doped cuprous oxide with copper vacancies: suppression of trap states, Chem. Mater. 25 (3) (2013) 253–265, https://doi.org/10.1021/cm3040278.

[19] F. Biccari. Defects and doping in Cu_2O, University of Rome, 2009. Doctoral dissertation.

[20] Y.S. Lee, J. Heo, M.T. Winkler, S.C. Siah, S.B. Kim, R.G. Gordon, T. Buonassisi, Nitrogen-doped cuprous oxide as a p-type hole-transporting layer in thin-film solar cells, J. Mater. Chem. A 1 (2013) 15416–15422, https://doi.org/10.1039/C3TA13208K.

[21] K.-S. Cho, D.-H. Kim, Y.-H. Kim, J. Nah, H.-K. Kim, Li-doped Cu_2O/ZnO heterojunction for flexible and semi-transparent piezoelectric nanogenerators, Ceram. Int. 43 (2) (2017) 2279–2287, https://doi.org/10.1016/j.ceramint.2016.10.208.

[22] K. Karlsen. Characterization of Li doped, magnetron sputtered Cu_2O thin films, University of Oslo, 2019. Masters thesis.

[23] M. Mayer, Improved physics in SIMNRA 7, Nucl. Instrum. Methods Phys. Res. Section B 332 (2014) 176–180, https://doi.org/10.1016/j.nimb.2014.02.056.

[24] K. Bergum, H.N. Riise, S.M. Gorantla, E. Monakhov, B.G. Svensson, Thin film Cu_2O for solar cell applications. 2016 IEEE 43rd Photovoltaic Specialists Conference (PVSC), 2016, pp. 2770–2773, https://doi.org/10.1109/PVSC.2016.7750156.

[25] Y. Wang, J. Ghanbaja, F. Soldera, P. Boulet, D. Horwat, F. Mücklich, J. Pierson, Controlling the preferred orientation in sputter-deposited Cu_2O thin films: influence of the initial growth stage and homoepitaxial growth mechanism, Acta Mater. 76 (2014) 207–212, https://doi.org/10.1016/j.actamat.2014.05.008.

[26] D. Dastan, P. Londhe, N. Chaure, Characterization of TiO_2 nanoparticles prepared using different surfactants by solgel method, Journal of Materials Science: Materials in Electronics 25 (2014) 3473–3479, https://doi.org/10.1007/s10854-014-2041-9.

[27] D. Dastan, Effect of preparation methods on the properties of titania nanoparticles solvothermal versus sol-gel, Appl. Phys. A 123 (2017) 699, https://doi.org/10.1007/s00339-017-1309-3.

[28] D. Dastan, N. Chaure, M. Kartha, Surfactants assisted solvothermal derived titania nanoparticles: synthesis and simulation, J Mater Sci 28 (2017) 7784–7796, https://doi.org/10.1007/s10854-017-6474-9.

[29] A. Jafari, M. Alam, S. Ziakhodadadian, Z. Shi, H. Garmestani, A. Weidenbach, Ş Ţălu, Statistical, morphological, and corrosion behavior of PECVD derived cobalt oxide thin films, J. Mater. Sci. 30 (2019) 21185–21198, https://doi.org/10.1007/s10854-019-02492-6.

[30] W.-D. Zhou, D. Dastan, J. Li, X.-T. Yin, Q. Wang, Discriminable sensing response behavior to homogeneous gases based on n-ZnO/p-NiO composites, Nanomaterials 10 (4) (2020) 785, https://doi.org/10.3390/nano10040785.

[31] K. Bergum, H.N. Riise, S. Gorantla, P.F. Lindberg, I.J.T. Jensen, A.E. Gunnæs, A. Galeckas, S. Diplas, B.G. Svensson, E. Monakhov, Improving carrier transport in

Cu_2O thin films by rapid thermal annealing, J. Phys 30 (7) (2018) 075702, https://doi.org/10.1088/1361-648x/aaa5f4.
[32] C. Malerba, F. Biccari, C. Leonor Azanza Ricardo, M. D'Incau, P. Scardi, A. Mittiga, Absorption coefficient of bulk and thin film Cu_2O, Solar Energy Mater. Solar Cells 95 (10) (2011) 2848–2854, https://doi.org/10.1016/j.solmat.2011.05.047.
[33] D. Dastan, Nanostructured anatase titania thin films prepared by sol-gel dip coating technique, J. At. Mol. Condens. MatterNano Phys. 2 (2) (2015) 109–114.
[34] D. Dastan, S. Panahi, N. Chaure, Characterization of titania thin films grown by dip-coating technique, J. Mater. Sci. 27 (2016) 12291–12296, https://doi.org/10.1007/s10854-016-4985-4.
[35] R. Shakoury, A. Arman, Ş Ţălu, D. Dastan, C. Luna, S. Rezaee, Stereometric analysis of TiO_2 thin films deposited by electron beam ion assisted, Opt. Quantum Electron. 52 (5) (2020) 270, https://doi.org/10.1007/s11082-020-02388-4.
[36] C. Van de Walle, Hydrogen as a cause of doping in zinc oxide, Phys. Rev. Lett. 85 (5) (2000) 1012–1015, https://doi.org/10.1103/PhysRevLett.85.1012.
[37] U. Ozgur, Y. Alivov, C. Liu, A. Teke, M. Reshchikov, S. Dogan, V. Avrutin, S. x, H. Morkoc, A comprehensive review of ZnO materials and devices, J. Appl. Phys. 98 (4) (2005), https://doi.org/10.1063/1.1992666.